INSTITUTE OF PHYSICS PUBLISHING JOURNAL OF PHYSICS: CONDENSED MATTER

J. Phys.: Condens. Matter **15** (2003) 3555–3566 PII: S0953-8984(03)60550-3

Quasielastic neutron scattering study of hydrogen motion in C15-type YMn_2H_x

A V Skripov[1], J C Cook[2], T J Udovic[2], M A Gonzalez[3], R Hempelmann[4] and V N Kozhanov[1]

[1] Institute of Metal Physics, Urals Branch of the Academy of Sciences, Ekaterinburg 620219, Russia
[2] NIST Center for Neutron Research, National Institute of Standards and Technology, Gaithersburg, MD 20899, USA
[3] Institut Laue-Langevin, F-38042 Grenoble, France
[4] Institut für Physikalische Chemie, Universität des Saarlandes, D-66041 Saarbrücken, Germany

E-mail: skripov@imp.uran.ru

Received 7 March 2003
Published 19 May 2003
Online at stacks.iop.org/JPhysCM/15/3555

Abstract

In order to study the mechanism and parameters of hydrogen diffusion in the cubic (C15-type) Laves phase YMn_2, we have performed quasielastic neutron scattering measurements in YMn_2H_x ($x = 0.4$, 0.65 and 1.26) over the temperature range 30–395 K. It is found that the diffusive motion of hydrogen in this system can be described in terms of two jump processes: the fast localized H motion with the jump rate τ_l^{-1} and the slower process with the rate τ_d^{-1} associated with H jumps leading to long-range diffusion. The ratio τ_d/τ_l at room temperature is close to 10^2. Our results suggest that the localized H motion in YMn_2H_x corresponds to back-and-forth jumps of hydrogen atoms within pairs of interstitial g (Y_2Mn_2) sites. The parameters of the long-range diffusion of hydrogen in the samples with different H content are found to be close to each other. In the range 210–395 K, the temperature dependences of τ_d^{-1} and the hydrogen diffusivity are reasonably described by the Arrhenius law with activation energies 0.18–0.22 eV.

1. Introduction

One of the most interesting features of hydrogen diffusion in Laves-phase intermetallic compounds is the coexistence of two frequency scales of H hopping [1–5]. It has been found that in a number of cubic (C15-type) Laves phases AB_2, where hydrogen atoms occupy only tetrahedral sites of g type (A_2B_2), the faster jump process corresponds to localized motion within the hexagons formed by g sites, and the slower process is associated with H jumps from one g-site hexagon to another [5–7]. The difference between the characteristic frequencies of these jump processes is believed to result from the difference between the g–g distances r_1

(within the hexagon) and r_2 (between the nearest hexagons). The value of r_2/r_1 is determined by the positional parameters of hydrogen atoms at g sites; these parameters are found to depend strongly on the ratio of the metallic radii R_A and R_B of the elements A and B [8, 9]. Previously H motion has been investigated only in C15-type compounds with $R_A/R_B \leqslant 1.25$, where $r_2/r_1 > 1$ (changing from 1.07 for $ZrCr_2H_x$ [6] to 1.45 for TaV_2H_x [5]). For compounds with $R_A/R_B > 1.35$, the g–g distance r_2 is expected to become shorter than r_1. This may lead to a qualitative change in the microscopic picture of H motion: the faster jump process is expected to be transformed into the back-and-forth jumps within *pairs* of g sites separated by r_2.

The aim of the present work is to study the parameters of hydrogen motion in C15-type YMn_2 with $R_A/R_B = 1.425$. According to the neutron diffraction measurements [10], at room temperature D atoms in YMn_2D_x with $x \leqslant 3.4$ occupy only g sites with the positional parameters $X_g = 0.324$–0.327 and $Z_g = 0.137$–0.141. The spatial arrangement of g sites in a C15-type lattice has been discussed previously (see, e.g., figures 5 and 6 of [5]). Using the structural data for $YMn_2D_{1.0}$ [10], we find that $r_1 = 1.40$ Å, $r_2 = 1.09$ Å and $r_2/r_1 = 0.78$. Thus, the YMn_2–H(D) system offers a good opportunity for observation of the microscopic picture of hydrogen motion corresponding to $r_2/r_1 < 1$. In the region of low hydrogen concentrations ($x \leqslant 1.2$), the YMn_2H_x system retains the homogeneous solid solution state with the C15-type host-lattice structure down to 245 K; below this temperature a number of structural and magnetic phase transitions are known to occur [11]. In this work we report the results of our quasielastic neutron scattering (QENS) measurements for YMn_2H_x ($x = 0.4$, 0.65 and 1.26) over the temperature range 30–395 K. These measurements have revealed that the mobility of hydrogen in YMn_2 is very high. Our results are consistent with the existence of localized H motion within pairs of g sites separated by $r_2 \approx 1.1$ Å.

2. Experimental details

The YMn_2 compound was prepared by arc melting high-purity Y and Mn in a helium atmosphere followed by an annealing in argon at 850 °C for 50 h. This procedure resulted in the formation of a single-phase intermetallic having the cubic C15-type structure with the lattice parameter $a = 7.680$ Å. Powdered YMn_2 samples were charged with hydrogen in a Sieverts-type vacuum system. The calculated amounts of H_2 gas were admitted to the system at room temperature. In order to ensure homogeneous distribution of hydrogen, the samples were additionally annealed at 200 °C for 5 h. QENS spectra were measured for three YMn_2H_x samples with $x = 0.4$, 0.65 and 1.26. According to x-ray diffraction analysis, at room temperature all these samples are single-phase solid solutions with the C15-type host lattice and $a = 7.770$ Å ($x = 0.4$), 7.784 Å ($x = 0.65$) and 7.884 Å ($x = 1.26$).

QENS measurements were performed on the disc-chopper time-of-flight spectrometer DCS (NIST Center for Neutron Research, Gaithersburg, MD) and on the high-resolution backscattering spectrometer IN10 (Institute Laue-Langevin, Grenoble). These two spectrometers complement each other with respect to resolution and the accessible range of energy transfer $\hbar\omega$, enabling one to probe hydrogen motion in the range of hopping rates 10^8–10^{12} s^{-1}. The experimental conditions including the temperature ranges, the incident neutron wavelengths λ_i, the energy resolution (FWHM) and the ranges of $\hbar\omega$ and Q (corresponding to the elastic momentum transfer $\hbar Q$) are listed in table 1. For measurements on the DCS, the powdered YMn_2H_x samples were placed into hollow-cylinder Al containers, and for measurements on the IN10 they were placed into flat Al containers oriented nearly perpendicular to the incident beam. The depth of the containers was 0.5 mm for $YMn_2H_{0.4}$ and $YMn_2H_{0.65}$ and 0.3 mm for $YMn_2H_{1.26}$. The scattering angles corresponding to the Bragg reflections were excluded from the analysis (DCS) or shielded by cadmium (IN10).

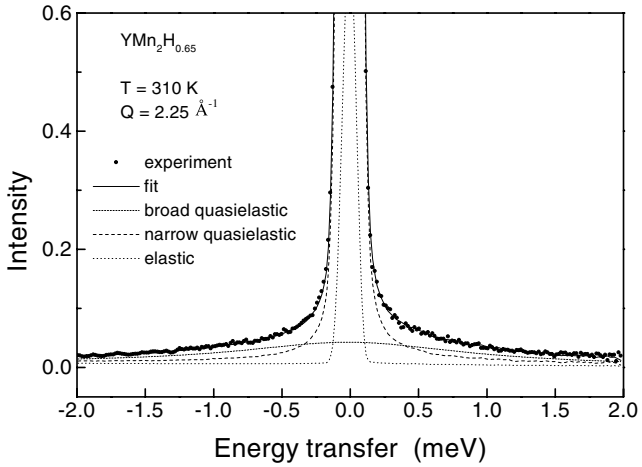

Figure 1. The QENS spectrum for $YMn_2H_{0.65}$ measured on DCS at $T = 310$ K and $Q = 2.25$ Å^{-1}. The full curve shows the fit of the three-component model (equation (1)) to the data. The dotted curve represents the spectrometer resolution function (the 'elastic' component), and the broken curves show two Lorentzian 'quasielastic' components.

Table 1. Experimental parameters for QENS measurements on YMn_2H_x.

Sample	Spectrometer	λ_i (Å)	T range (K)	Resolution (μeV)	$\hbar\omega$ range (meV)	Q range (Å^{-1})
$YMn_2H_{0.4}$	DCS	4.8	90, 260–395	120	±1.2	0.83–2.38
	IN10	6.27	30, 190–259	1.0	±0.0123	0.50–1.96
$YMn_2H_{0.65}$	DCS	4.8	70, 290–390	120	±2.0	0.54–2.25
	IN10	6.27	30, 190–259	1.0	±0.0123	0.50–1.96
$YMn_2H_{1.26}$	IN10	6.27	30, 210–259	1.0	±0.0123	0.50–1.96

The raw experimental data were corrected for absorption and self-shielding using the standard NIST or ILL programs. For both spectrometers, the instrumental resolution functions were determined from the measured QENS spectra of YMn_2H_x at low temperatures (70 and 90 K for the DCS and 30 K for the IN10). The background spectra were measured for the empty sample containers in the same experimental geometry as for YMn_2H_x.

3. Results and discussion

3.1. Time-of-flight QENS spectra

QENS spectra for $YMn_2H_{0.4}$ and $YMn_2H_{0.65}$ measured on DCS in the temperature range 260–395 K can be satisfactorily described by a sum of three components: an elastic line represented by the spectrometer resolution function $R(Q, \omega)$ and two resolution-broadened Lorentzian quasielastic lines with different widths. As an example of the data, figure 1 shows the QENS spectrum of $YMn_2H_{0.65}$ recorded at 310 K for $Q = 2.25$ Å^{-1}. It should be noted that time-of-flight QENS spectra for C15-type TaV_2H_x [5], $ZrMo_2H_x$ [7] and $HfMo_2H_x$ [8] over the same temperature range are well described by a sum of an elastic line and a single Lorentzian quasielastic component. However, attempts to use a similar model for YMn_2H_x have been found to result in systematic deviations of the model spectra from the experimental ones. Thus, the third component appears to be crucial for a reasonable description of the QENS spectra

for YMn_2H_x. As can be seen from figure 1, one of the Lorentzian quasielastic lines is quite narrow and the other one is very broad. We have fitted the experimental scattering function $S_{exp}(Q, \omega)$ with the model incoherent scattering function:

$$S_{inc}(Q, \omega) = A_0(Q)\delta(\omega) + A_1(Q)L(\omega, \Gamma_1) + A_2(Q)L(\omega, \Gamma_2) \quad (1)$$

convoluted with $R(Q, \omega)$. Here $\delta(\omega)$ is the elastic δ-function, $L(\omega, \Gamma)$ is the quasielastic Lorentzian with the half-width Γ and $A_0 + A_1 + A_2 = 1$. As the first step of the analysis, we have used the model function (1) with all the amplitudes (A_0, A_1, A_2) and the half-widths (Γ_1, Γ_2) being independent fit parameters. Qualitatively, the results of such an analysis are similar for both $YMn_2H_{0.4}$ and $YMn_2H_{0.65}$. The intensity of the broad quasielastic component, $A_2(Q)$, is found to increase with increasing Q; however, it remains small over the whole studied Q range. The half-width of this component, Γ_2, is found to be nearly Q-independent. These features are typical of the case of spatially confined (localized) motion [12, 13], the value of Γ_2 being proportional to the hopping rate τ_l^{-1}. Therefore, the broad quasielastic component (the third term in equation (1)) can be ascribed to the fast localized H motion. In order to obtain information on the geometry of this motion, we have to analyse the Q dependence of A_2. The narrow quasielastic line appears to be the dominant component of the spectra. Its half-width Γ_1 is found to increase with increasing Q, reaching a saturation in the Q range 1.6–2.2 $Å^{-1}$. Furthermore, the value of Γ_1 increases strongly with increasing temperature. These features suggest that the narrow quasielastic component originates from a jump process leading to the long-range diffusion of hydrogen. The intensity of the elastic component, A_0, is found to be small (about 10% of the total scattered intensity), being nearly Q- and T-independent. This component can be attributed to the residual elastic contribution resulting mainly from the scattering by host-metal nuclei.

Since A_0 and Γ_2 appear to be nearly Q-independent, the values of these parameters have been fixed for the next step of the analysis. Thus, only A_1 and Γ_1 remain to be independent fit parameters, the value of A_2 being determined as $1 - A_0 - A_1$. In this case the fitting procedure becomes quite stable. An additional complication arises from the very large half-width of the broad quasielastic component combined with its small intensity. For example, the value of Γ_2 for $YMn_2H_{0.65}$ at $T = 310$ K is found to be equal to 0.98 meV. For comparison, the half-width of the broad quasielastic component for $TaV_2H_{0.6}$ (having the fastest localized H motion among the Laves-phase hydrides studied previously) at $T = 300$ K is 0.24 meV [5]. Because of the very large Γ_2, the broad quasielastic line for YMn_2H_x can be reliably separated from the flat background only at the low end of the temperature range of our measurements (i.e. at temperatures close to 300 K). At higher temperatures, where Γ_2 is expected to become larger, such a separation is problematic. In order to evaluate A_1 and Γ_1 at all temperatures, we have fixed the values of Γ_2 at $T > 310$ K to the corresponding values of Γ_2 near room temperature ($\Gamma_2(290\ K) = 0.74$ meV for $YMn_2H_{0.4}$ and $\Gamma_2(310\ K) = 0.98$ meV for $YMn_2H_{0.65}$). Because of the large difference between the values of Γ_1 and Γ_2, this simplification should not strongly affect the parameters of the narrow quasielastic component. On the other hand, this simplification does not allow us to analyse the details of the localized H motion at high temperatures. The parameters of hydrogen motion resulting from our analysis will be discussed in section 3.3.

3.2. Backscattering QENS spectra

QENS spectra for YMn_2H_x measured on IN10 in the temperature range 210–259 K can be reasonably described by a sum of an elastic line and a resolution-broadened quasielastic line. For all the samples studied, the quasielastic component has not been detected below 200 K. As

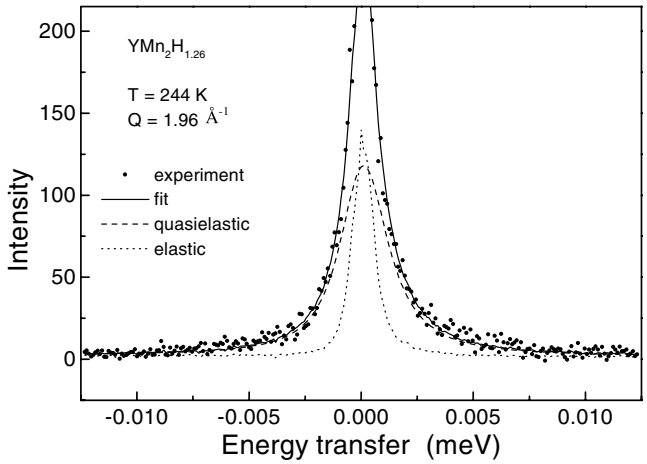

Figure 2. The QENS spectrum for $YMn_2H_{1.26}$ measured on IN10 at $T = 244$ K and $Q = 1.96$ Å^{-1}. The full curve shows the fit of the two-component model to the data. The dotted curve represents the spectrometer resolution function (the 'elastic' component), and the broken curve shows the Lorentzian 'quasielastic' component.

an example of the data, figure 2 shows the QENS spectrum of $YMn_2H_{1.26}$ recorded at 244 K for $Q = 1.96$ Å^{-1}. The half-width of the Lorentzian quasielastic component is found to increase with increasing Q, reaching a saturation in the Q range 1.5–2.0 Å^{-1}. Such a behaviour is typical of the case of a jump process leading to long-range diffusion [12, 13]. Therefore, this quasielastic line is likely to originate from the same process as the narrow quasielastic line in the time-of-flight QENS spectra. The quantitative analysis to be presented in section 3.3 confirms this assumption.

The broader quasielastic line has not been found in the backscattering QENS spectra. Most probably, this results from a combination of a narrow energy transfer range of IN10 and a low intensity of the broader line. Under these conditions it is extremely difficult to distinguish between the broad quasielastic line and the flat background.

3.3. Parameters of hydrogen motion

Examples of the Q dependence of the half-width of the narrow quasielastic line, as derived from the QENS spectra measured on DCS and IN10, are shown in figures 3 and 4, respectively. For the other YMn_2H_x samples studied, the $\Gamma_1(Q)$ have similar shapes. For parametrization of these dependences, we have used the orientationally averaged Chudley–Elliott model [14]. The corresponding form of $\Gamma_1(Q)$ is

$$\Gamma_1(Q) = \frac{\hbar}{\tau_d}\left(1 - \frac{\sin QL}{QL}\right), \tag{2}$$

where τ_d is the mean time between two successive H jumps leading to long-range diffusion, and L is the effective jump length. The fits of equation (2) to the data are shown by the full curves in figures 3 and 4. The temperature dependences of the jump rates τ_d^{-1} resulting from the Chudley–Elliott fits are presented in figure 5. As can be seen from this figure, the values of τ_d^{-1} derived from the measurements on DCS and IN10 are likely to originate from the same motional process described by the Arrhenius law

$$\tau_d^{-1} = \tau_{d0}^{-1} \exp(-E_a/k_B T), \tag{3}$$

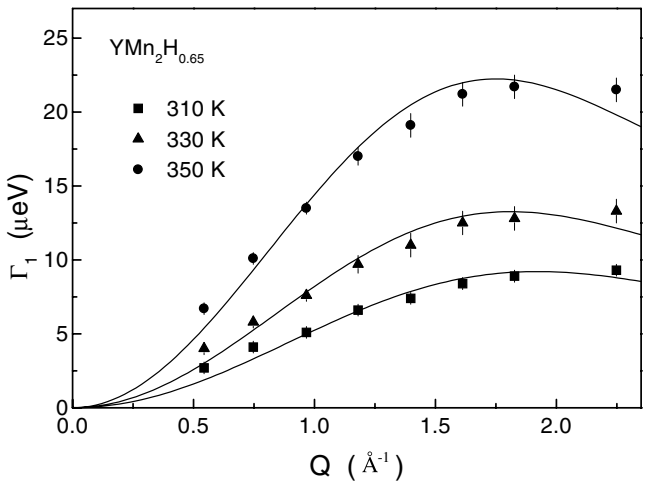

Figure 3. The half-width (HWHM) of the narrow Lorentzian QENS component for $YMn_2H_{0.65}$ as a function of Q measured on DCS at $T = 310$, 330 and 350 K. The full curves show the fits of the Chudley–Elliott model (equation (2)) to the data.

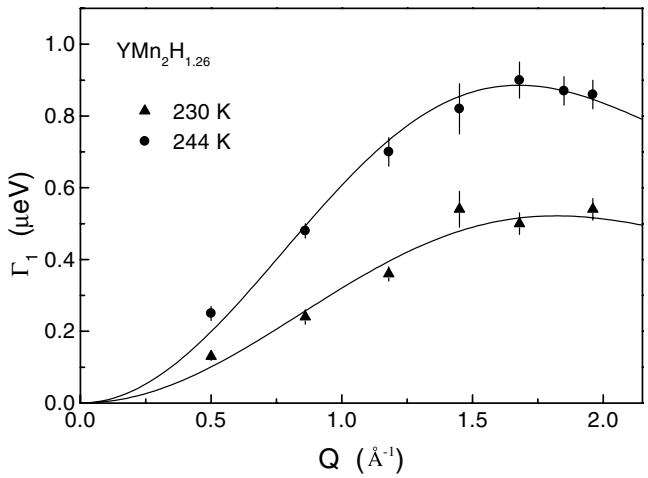

Figure 4. The half-width (HWHM) of the narrow Lorentzian QENS component for $YMn_2H_{1.26}$ as a function of Q measured on IN10 at $T = 230$ and 244 K. The full curves show the fits of the Chudley–Elliott model (equation (2)) to the data.

where E_a is the activation energy for hydrogen diffusion. According to [11], at $T \approx 245$ K both $YMn_2H_{0.4}$ and $YMn_2H_{0.65}$ show transitions from the cubic (α) phase to the tetragonally distorted (β') phase. The data presented in figure 5 indicate that these phase transitions are not accompanied by strong changes in the parameters of hydrogen motion. The full line in figure 5 shows the global Arrhenius fit to the τ_d^{-1} data for $YMn_2H_{0.65}$ (including both the DCS and IN10 results); the corresponding fit parameters are $E_a = 213 \pm 5$ meV and $\tau_{d0}^{-1} = (2.9 \pm 0.5) \times 10^{13}$ s^{-1}. The analogous Arrhenius fit to the τ_d^{-1} data for $YMn_2H_{0.4}$ yields $E_a = 190 \pm 7$ meV and $\tau_{d0}^{-1} = (8 \pm 2) \times 10^{12}$ s^{-1}.

The average values of L resulting from the Chudley–Elliott fits are 2.4 Å for $YMn_2H_{0.4}$, 2.5 Å for $YMn_2H_{0.65}$ and 2.6 Å for $YMn_2H_{1.26}$. These values are considerably longer than

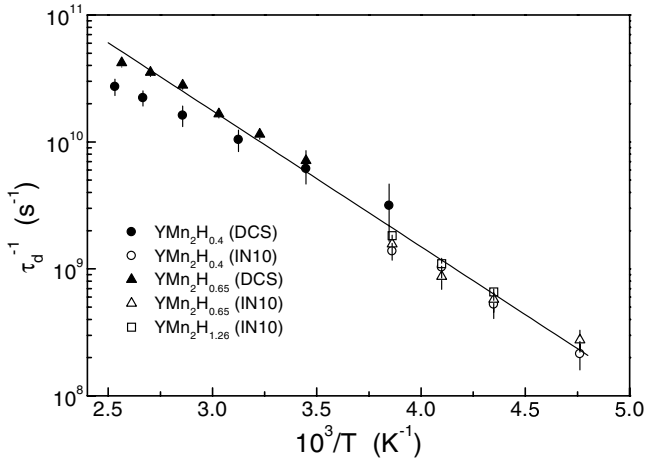

Figure 5. The temperature dependence of the hydrogen jump rates τ_d^{-1} derived from the Chudley–Elliott fits (equation (2)). The full line shows the global Arrhenius fit to the data for $YMn_2H_{0.65}$.

the distances r_1 and r_2 between the nearest-neighbour g sites ($r_1 = 1.39$ Å, $r_2 = 1.08$ Å for $YMn_2H_{0.65}$). The values of L exceeding 2 Å have also been reported previously for a number of cubic Laves phase hydrides with g-site occupation [5, 6, 15–18]. This feature can be accounted for in terms of the model implying two frequency scales of H motion: the jump rate for localized motion, τ_l^{-1}, and the jump rate responsible for long-range diffusion, τ_d^{-1}, with $\tau_d^{-1} \ll \tau_l^{-1}$. As explained in [5, 6], in this model τ_d is the mean residence time of a hydrogen atom at a group of sites connected by the localized motion. Since an H atom may enter such a group through one site and leave it from the other site, the total displacement for the time τ_d is expected to be larger than the distance between the nearest-neighbour sites. If the localized H motion occurs within pairs of g sites separated by r_2, a rough estimate of L is given by the distance between the centres of such adjacent pairs. For the studied YMn_2H_x compounds, this distance is about 2.0 Å.

The relation between the tracer diffusion coefficient D and the values of τ_d and L is given by

$$D = \frac{L^2}{6\tau_d}. \tag{4}$$

We assume here that the tracer correlation factor [19] for H diffusion is equal to 1. This assumption is well justified, since in our samples less than 11% of all available g sites are occupied by hydrogen. Using the values of τ_d and L derived from the Chudley–Elliott fits, we can obtain D from equation (4). The resulting D values are shown in figure 6. The full line in this figure represents the global Arrhenius fit to the DCS and IN10 data for $YMn_2H_{0.65}$; the corresponding fit parameters are the activation energy $E_a = 209 \pm 6$ meV and the pre-exponential factor $D_0 = (2.9 \pm 0.6) \times 10^{-3}$ cm^2 s^{-1}. For $YMn_2H_{0.4}$, the global Arrhenius fit yields $E_a = 178 \pm 7$ meV and $D_0 = (5.9 \pm 1.7) \times 10^{-4}$ cm^2 s^{-1}.

We now turn to a discussion of the parameters of the faster jump process associated with localized H motion. In order to elucidate the geometry of the localized H motion, we have to analyse the behaviour of the elastic incoherent structure factor (EISF) [12, 13] as a function of Q. As noted in section 3.1, because of the large width of the broader quasielastic component, the appropriate analysis is only possible at the low-T end of our experimental range of time-of-flight QENS measurements. For QENS spectra described by equation (1),

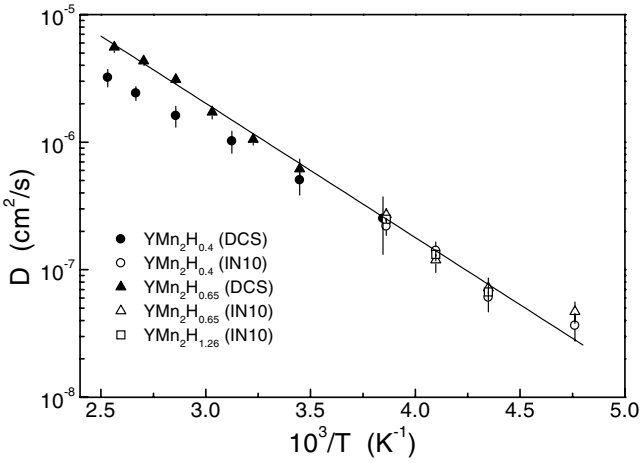

Figure 6. The temperature dependence of the tracer diffusion coefficients of hydrogen derived from the Chudley–Elliott fits (equations (2) and (4)). The full line shows the global Arrhenius fit to the data for $YMn_2H_{0.65}$.

the 'resolution-limited' EISF is defined as $(A_0 + A_1)/(A_0 + A_1 + A_2) = A_0 + A_1$. Assuming that the purely elastic component of the observed QENS spectra originates from the host-metal contribution to the incoherent scattering function, we can conclude that the EISF for the hydrogen sublattice is determined by the ratio $A_1/(A_1 + A_2)$. Figure 7 shows this ratio as a function of Q for $YMn_2H_{0.65}$ at $T = 310$ K. Taking into account that only a fraction $p(T)$ of H atoms may participate in the localized motion [5], the orientationally averaged form of the EISF for the hopping within pairs of sites separated by a distance d [12, 13] is given by

$$\text{EISF} = 1 - p + \frac{p}{2}[1 + j_0(Qd)], \tag{5}$$

where $j_0(x)$ is the spherical Bessel function of zeroth order. The fit of equation (5) to the data shown in figure 7 yields $p = 0.39 \pm 0.03$ and $d = 1.17 \pm 0.09$ Å. Note that the fitted value of d is close to the distance between the nearest-neighbour g sites in $YMn_2H_{0.65}$, $r_2 = 1.08$ Å. Thus, the observed Q dependence of the EISF in $YMn_2H_{0.65}$ is consistent with the localized motion within pairs of g sites. The fit of equation (5) with the fixed value $d = 1.08$ Å to the data gives $p = 0.44 \pm 0.01$. This fit is shown by the full curve in figure 7. The alternative model of localized H motion implies hopping within the hexagons formed by g sites [5]. If r is the distance between the nearest-neighbour sites in the hexagons, the fit of the six-site model to the data shown in figure 7 yields $p = 0.156 \pm 0.003$ and $r = 1.19 \pm 0.03$ Å. The fitted value of r is smaller than the corresponding value resulting from the structure of $YMn_2H_{0.65}$, $r_1 = 1.39$ Å. Thus, the two-site model appears to be preferable. The Q dependence of the EISF for $YMn_2H_{0.4}$ at $T = 290$ K is very close to that for $YMn_2H_{0.65}$.

It should be noted, however, that because of the weakness of the observed Q dependence of the EISF, the results presented in figure 7 cannot be considered as a proof of the two-site localized motion. In fact, the available experimental Q range (with the maximum Q value of 2.25 Å^{-1}) is not sufficient to trace the EISF described by equation (5) to the first minimum of the Bessel function. Thus, we can only state that the observed Q dependence of the EISF is consistent with the two-site model. An additional argument in favour of the two-site model is the large width of the broader quasielastic component for YMn_2H_x. As noted in section 3.1, the value of Γ_2 for $YMn_2H_{0.65}$ at 310 K appears to be nearly 4 times higher than that for

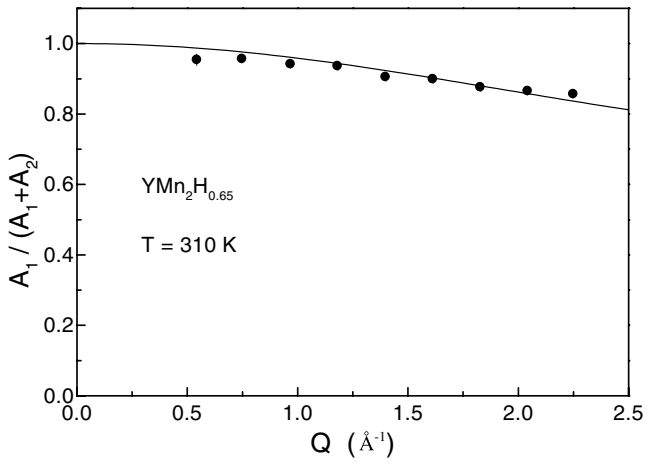

Figure 7. The EISF for $YMn_2H_{0.65}$ at 310 K as a function of Q. The full curve shows the fit of the two-site model (equation (5)) with the fixed $d = 1.08$ Å to the data.

$TaV_2H_{0.6}$, while the nearest-neighbour g–g distances in these compounds are close to each other. This feature may be accounted for by different relations between the jump rate and the quasielastic linewidth for the two-site and six-site models of localized motion. According to [12], for the two-site model $\Gamma_2 = 2\hbar\tau_l^{-1}$, while for the six-site model $\Gamma_2 \approx 0.55\hbar\tau_l^{-1}$ (being slightly Q-dependent). This means that, for the same jump rate, the quasielastic linewidth for the two-site localized motion is expected to be considerably larger than for the six-site motion.

3.4. Comparison with other Laves-phase hydrides

In order to discuss the systematics of H motion in cubic Laves phases, it is useful to compare the results for YMn_2H_x with those for other isomorphous AB_2H_x compounds. First, we shall consider the relation between R_A/R_B and the structure of the g-site sublattice. The value of the g–g distance ratio r_2/r_1 is determined by the positional parameters (X_g and Z_g) of hydrogen atoms at g sites. Since g sites are coordinated by 2 A and 2 B atoms, one may expect that the positional parameters X_g and Z_g (and hence r_2/r_1) are related to R_A/R_B. In order to verify this, we have analysed the available neutron diffraction data for paramagnetic C15-type deuterides AB_2D_x, where both A and B are transition metals. The results are presented in figure 8. In the cases where the neutron diffraction data are available for different deuterium concentrations x, we have used the positional parameters X_g and Z_g corresponding to lower x. It should be noted that the changes in X_g and Z_g with x are considerably smaller than the range of variation of these parameters for different Laves-phase compounds. As can be seen from figure 8, there is a clear correlation between r_2/r_1 and R_A/R_B for cubic Laves-phase hydrides and the data for YMn_2–H(D) are consistent with this correlation. These results show that, although the structure of the host-metal lattice is the same for cubic Laves-phase hydrides, the structure of the g-site hydrogen sublattice changes strongly as a function of R_A/R_B.

We now turn to a discussion of the relation between the intersite distances and the jump rates. Since the ratio of the jump rates τ_d/τ_l depends on temperature, we have to choose a certain temperature for comparison of the data. At $T < 200$ K the value of τ_d^{-1} in Laves-phase hydrides (except for $ZrCr_2H_x$) becomes too low to be determined from QENS and nuclear spin-lattice relaxation (NSLR) measurements. On the other hand, at room temperature both τ_l^{-1} and τ_d^{-1} can be measured (the former from the time-of-flight QENS and the latter mostly

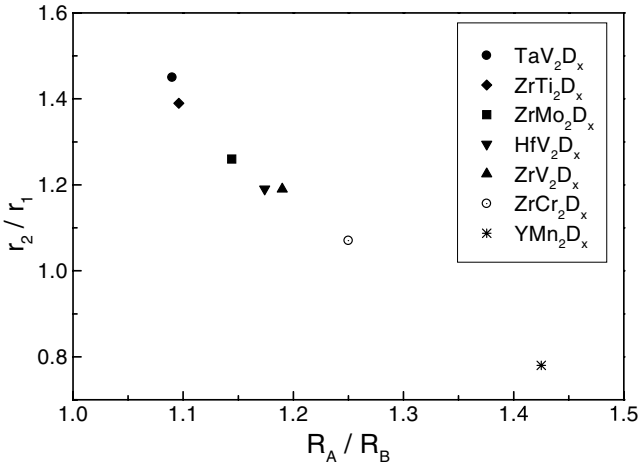

Figure 8. The ratio of the g–g distances as a function of R_A / R_B for a number of C15-type deuterides AB_2D_x. The values of r_1 / r_2 are derived from the neutron diffraction data for TaV_2D_x [20], $ZrTi_2D_x$ [21], $ZrMo_2D_x$ [22], HfV_2D_x [23], ZrV_2D_x [24], $ZrCr_2D_x$ [25] and YMn_2D_x [10].

from the backscattering QENS and NSLR). At present, the measured values of both τ_l^{-1} and τ_d^{-1} are available for TaV_2H_x [4, 5], $ZrCr_2H_x$ [6, 26], $ZrMo_2H_x$ [7], $HfMo_2H_x$ [8, 27] and ZrV_2H_x [18, 28]. In table 2, the g–g distances r_1 and r_2 and the hydrogen jump rates at 300 K for $YMn_2H_{0.65}$ are compared with the corresponding values for C15-type $TaV_2H_{1.1}$, $HfMo_2H_{0.26}$, $ZrMo_2H_{0.92}$, $ZrV_2H_{1.1}$ and $ZrCr_2H_{0.45}$. Also included in table 2 are the values of hydrogen diffusivity at 300 K and the activation energy of the slower jump process. All the motional parameters for hydrogen in $YMn_2H_{0.65}$ result from the present work. The values of $\tau_l^{-1}(300\ \mathrm{K})$ are obtained from the time-of-flight QENS data for $TaV_2H_{1.1}$ [5], $HfMo_2H_{0.26}$ [8], $ZrMo_2H_{0.92}$ [7], $ZrV_2H_{1.1}$ [18] and $ZrCr_2H_{0.5}$ [29]. The values of $\tau_d^{-1}(300\ \mathrm{K})$ are estimated from the NSLR measurements on $TaV_2H_{1.15}$ [4], $HfMo_2H_{0.4}$ [27], $ZrMo_2H_{1.0}$ [7] and $ZrV_2H_{1.1}$ [28], and from the backscattering QENS data for $ZrCr_2H_{0.45}$ [6]. The values of H diffusivity at 300 K are obtained from the backscattering QENS results for $TaV_2H_{1.1}$ [5] and $ZrCr_2H_{0.45}$ [6], and from the pulsed-field-gradient NMR data for $ZrMo_2H_{0.9}$ and $ZrV_2H_{1.0}$ [30]. The activation energies E_a for the slower jump process are derived from the NSLR measurements on $TaV_2H_{1.15}$ [4], $HfMo_2H_{0.4}$ [27], $ZrMo_2H_{0.5}$ [7], $ZrV_2H_{1.1}$ [28] and $ZrCr_2H_{0.5}$ [26, 31]. It should be noted that the E_a values in table 2 describe the temperature dependence of τ_d^{-1} above 200 K. As explained in [6], in some cases these values may differ from those describing the temperature dependence of D in the same range. Such a difference is quite large for $ZrCr_2H_x$ due to the temperature dependence of the effective L value [6]: the measured values of E_a for the tracer diffusion coefficient above 200 K are 137 meV in $ZrCr_2H_{0.5}$ [30] and 136 meV in $ZrCr_2H_{0.45}$ [6], to be compared with 84 meV in table 2.

As can be seen from table 2, the values of both $\tau_l^{-1}(300\ \mathrm{K})$ and $\tau_d^{-1}(300\ \mathrm{K})$ for $YMn_2H_{0.65}$ are higher than the corresponding values for the other studied C15-type hydrides. The tracer diffusion coefficient of hydrogen in $YMn_2H_{0.65}$ at room temperature also appears to be the highest among the Laves-phase hydrides studied. However, at $T < 250$ K the hydrogen diffusivity for $YMn_2H_{0.65}$ becomes lower than that for $ZrCr_2H_{0.45}$; this is related to the very small value of E_a for $ZrCr_2H_x$. For the compounds with $r_2/r_1 > 1$, there are clear correlations between r_1 and $\tau_l^{-1}(300\ \mathrm{K})$ and between r_2 and $\tau_d^{-1}(300\ \mathrm{K})$, the increase in intersite distances leading to a decrease in the corresponding jump rates. The results for YMn_2H_x should be considered, keeping in mind that in this case the expected relations are between r_1 and τ_d^{-1} and

Table 2. The intersite distances and the parameters of hydrogen motion at 300 K for cubic Laves-phase hydrides. See the text for details and sources of the data.

Parameter	$TaV_2H_{1.1}$	$HfMo_2H_{0.26}$	$ZrMo_2H_{0.92}$	$ZrV_2H_{1.1}$	$ZrCr_2H_{0.45}$	$YMn_2H_{0.65}$
r_1 (Å)	0.99	1.10	1.12	1.15	1.13	1.39
r_2 (Å)	1.44	1.39	1.41	1.37	1.21	1.08
r_2/r_1	1.45	1.26	1.26	1.19	1.07	0.78
τ_l^{-1} (300 K) (s^{-1})	3.8×10^{11}	1.6×10^{11}	1.1×10^{11}	1.6×10^{11}	7.1×10^{10}	7.4×10^{11}
τ_d^{-1} (300 K) (s^{-1})	7.3×10^{7}	6.6×10^{7}	5.7×10^{7}	6.7×10^{8}	3.5×10^{9}	7.7×10^{9}
τ_d/τ_l (300 K)	5.2×10^{3}	2.4×10^{3}	1.9×10^{3}	240	20	96
D (300 K) ($cm^2\ s^{-1}$)	2.2×10^{-8}		2.7×10^{-8}	1.2×10^{-7}	6.3×10^{-7}	8.9×10^{-7}
E_a (meV)	220	260	230	160	84	213

between r_2 and τ_l^{-1}. Nevertheless, the data for YMn_2H_x do not follow the same trends as the data for compounds with $r_2/r_1 > 1$. Apart from possible reasons of electronic origin, this may be associated with the geometry of the g-site sublattice. In fact, each g-site has three nearest neighbours: two at a distance r_1 and one at a distance r_2 (see, e.g., figures 5 and 6 of [5]). While for compounds with $r_2/r_1 > 1$ only one jump direction leads to the long-range diffusion, for YMn_2H_x there are two jump directions which are expected to lead to the long-range diffusion. Therefore, for YMn_2H_x (and other C15-type compounds with $r_2/r_1 < 1$) the long-range H diffusion should be relatively faster than in compounds with $r_2/r_1 > 1$, and the jump rate ratio τ_d/τ_l should be smaller than that expected on the basis of the r_2/r_1 value. This is consistent with our results for YMn_2H_x.

4. Conclusions

The analysis of our QENS data for C15-type YMn_2H_x has shown that the diffusive motion of hydrogen in this system can be described in terms of at least two jump processes with different frequency scales. The faster process with the jump rate τ_l^{-1} corresponds to localized H motion, and the slower process with the jump rate τ_d^{-1} is associated with H jumps leading to long-range diffusion. The ratio of the jump rates for these two processes, τ_d/τ_l, at room temperature is found to be close to 10^2. Our results suggest that the geometry of the localized H motion in YMn_2H_x differs from that found in the other C15-type hydrides studied previously; the experimental data for YMn_2H_x are consistent with back-and-forth jumps of hydrogen atoms within pairs of g sites.

The long-range mobility of hydrogen in YMn_2H_x is found to be very high. In fact, at room temperature the values of both τ_d^{-1} and the tracer diffusion coefficient D derived from our data for YMn_2H_x ($x = 0.4$ and 0.65) are higher than the corresponding values for the other studied Laves-phase hydrides. The temperature dependences of τ_d^{-1} and D in the range 210–395 K can be reasonably described by the Arrhenius law with the activation energies 190 ± 7 meV (τ_d^{-1} for $YMn_2H_{0.4}$) and 213 ± 5 meV (τ_d^{-1} for $YMn_2H_{0.65}$). The values of τ_d^{-1} and D for $YMn_2H_{1.26}$ in the studied range 230–260 K are found to be close to the corresponding values for $YMn_2H_{0.4}$ and $YMn_2H_{0.65}$.

Acknowledgments

This work was supported by the NATO Linkage grant no HTECH.LG 973890. The facilities used in this work were supported in part by the National Science Foundation under agreement no DMR-0086210.

References

[1] Bowman R C, Craft B D, Attalla A and Johnson J R 1983 *Int. J. Hydrog. Energy* **8** 801
[2] Hempelmann R, Richter D and Heidemann A 1982 *J. Less-Common Met.* **88** 343
[3] Skripov A V, Belyaev M Yu, Rychkova S V and Stepanov A P 1989 *J. Phys.: Condens. Matter* **1** 2121
[4] Skripov A V, Rychkova S V, Belyaev M Yu and Stepanov A P 1990 *J. Phys.: Condens. Matter* **2** 7195
[5] Skripov A V, Cook J C, Sibirtsev D S, Karmonik C and Hempelmann R 1998 *J. Phys.: Condens. Matter* **10** 1787
[6] Skripov A V, Pionke M, Randl O and Hempelmann R 1999 *J. Phys.: Condens. Matter* **11** 1489
[7] Skripov A V, Cook J C, Karmonik C and Kozhanov V N 1999 *Phys. Rev.* B **60** 7238
[8] Skripov A V, Cook J C, Udovic T J and Kozhanov V N 2000 *Phys. Rev.* B **62** 14099
[9] Skripov A V, Cook J C, Udovic T J, Kozhanov V N and Hempelmann R 2002 *Appl. Phys. (Suppl.1)* A **74** S948
[10] Latroche M, Paul-Boncour V, Przewoznik J, Percheron-Guégan A and Bourée-Vigneron F 1995 *J. Alloys Compounds* **231** 99
[11] Figiel H, Przewoznik J, Paul-Boncour V, Lindbaum A, Gratz E, Latroche M, Escorne M, Percheron-Guégan and Mietniowski P 1998 *J. Alloys Compounds* **274** 29
[12] Bée M 1988 *Quasielastic Neutron Scattering* (Bristol: Hilger)
[13] Hempelmann R 2000 *Quasielastic Neutron Scattering and Solid State Diffusion* (Oxford: Clarendon)
[14] Chudley C T and Elliott R J 1961 *Proc. Phys. Soc.* **77** 353
[15] Havill R L, Titman J M, Wright M S and Crouch M A 1989 *Z. Phys. Chem. Neue Folge* **164** 1083
[16] Schönfeld C 1992 *PhD Thesis* Technische Hochschule Aachen
[17] Campbell S I, Kemali M, Ross D K, Bull D J, Fernandez J F and Johnson M R 1999 *J. Alloys Compounds* **293–295** 351
[18] Bull D J 2001 *PhD Thesis* University of Salford
[19] Tahir-Kheli R A and Elliott R J 1983 *Phys. Rev.* B **27** 844
[20] Fischer P, Fauth F, Skripov A V, Podlesnyak A A, Padurets L N, Shilov A L and Ouladdiaf B 1997 *J. Alloys Compounds* **253/254** 282
[21] Skripov A V, Udovic T J, Huang Q, Cook J C and Kozhanov V N 2000 *J. Alloys Compounds* **311** 234
[22] Fischer P, Fauth F, Skripov A V and Kozhanov V N 2003 at press
[23] Irodova A V, Glazkov V P, Somenkov V A and Shil'shtein S Sh 1980 *Sov. Phys.–Solid State* **22** 45
[24] Didisheim J J, Yvon K, Shaltiel D, Fischer P, Bujard P and Walker E 1979 *Solid State Commun.* **32** 1087
[25] Kohlmann H, Fauth F, Fischer P, Skripov A V, Kozhanov V N and Yvon K 2001 *J. Alloys Compounds* **327** L4
[26] Skripov A V and Belyaev M Yu 1993 *J. Phys.: Condens. Matter* **5** 4767
[27] Skripov A V, Soloninin A V, Stepanov A P and Kozhanov V N 1999 *J. Phys.: Condens. Matter* **11** 10393
[28] Skripov A V, Belyaev M Yu, Rychkova S V and Stepanov A P 1991 *J. Phys.: Condens. Matter* **3** 6277
[29] Skripov A V, Cook J C and Udovic T J 1999 unpublished results
[30] Majer G, Renz W, Seeger A, Barnes R G, Shinar J and Skripov A V 1995 *J. Alloys Compounds* **231** 220
[31] Stoddard R D and Conradi M S 1998 *Phys. Rev.* B **57** 10455